Tectonophysics 887 (2024) 230455

Contents lists available at ScienceDirect

Tectonophysics

journal homepage: www.elsevier.com/locate/tecto

Upper-mantle seismic anisotropy in the southwestern North Island, New Zealand: Implications for regional upper-mantle and slab deformation

Lingmin Cao [a,b,*], Xiaobo He [c,**], Huaiyu Yuan [d,e], Minghui Zhao [a,b,f], Xuelin Qiu [a,b,f], Martha K. Savage [g]

[a] Key Laboratory of Ocean and Marginal Sea Geology, South China Sea Institute of Oceanology, Chinese Academy of Sciences, China
[b] Southern Marine Science and Engineering Guangdong Laboratory, Guangzhou, China
[c] Department of Ocean Exploration and Technology, Zhejiang Ocean University, Zhoushan, China
[d] Geological Survey of Western Australia, East Perth, Western Australia, Australia
[e] Centre for Exploration Targeting, University of Western Australia, Australia
[f] University of Chinese Academy of Sciences, China
[g] School of Geography, Environment and Earth Sciences, Victoria University of Wellington, Wellington, New Zealand

ARTICLE INFO

Keywords:
New Zealand
Seismic anisotropy
Dynamics of lithosphere and mantle

ABSTRACT

We employed shear-wave splitting analysis on both teleseismic *SKS* and *S* waves, and *S* waves from deep (150–250 km) local earthquakes collected from a dense array with 43 temporary broadband seismic stations and nine long-term seismic stations centered at Mount Taranaki to characterize the upper-mantle dynamics in the southwestern North Island of New Zealand, in areas previously unexamined for shear-wave splitting. We observed predominantly trench-parallel fast polarizations and strikingly large delay times over 3 s from teleseismic analysis. In contrast, local *S* analysis yielded a sharp transition of fast-polarization from trench-parallel in the northeast to trench-normal in the southwest. Trench-parallel fast-polarization from teleseismic analysis may be attributed to sub-slab trench-parallel flow or to trench-parallel fractures in the subducting slab. More importantly, we attribute large delay times to deep upper-mantle (200–400 km depth) deformation, possibly associated with the dynamic interaction between the downgoing slab and the 410-km discontinuity or with the lithosphere delamination near the Taranaki-Ruapehu line. In contrast, the trench-parallel anisotropy from the local *S* waves in the northeast could be caused by fluid-bearing cracks in the crust of the Taupō Volcanic Zone and/or by trench-parallel fractures in the subducting slab resulting from outer rise bending. The abrupt change to trench-normal may be related to stress variations in the downgoing slab at different depths.

1. Introduction

The North Island of New Zealand is located above the Hikurangi subduction zone, where the Pacific plate has been subducting beneath the Australian plate with a convergence rate of ~40–45 mm/yr at an oblique angle to the strike of the plate boundary (DeMets et al., 2010; Fig. 1). Subduction of the Pacific plate initiated at the Hikurangi margin at ca. 25 Ma and then rotated clockwise with time (rotation rate ~ 3°/Ma; e.g., Walcott, 1987; Wallace et al., 2004; Nicol et al., 2007). Seismic evidence suggests that the slab reaches a depth of >300 km (Williams et al., 2013; Fig. 1). The depth contours of the upper boundaries of the subducting Pacific slab beneath the North Island are mostly smooth (Williams et al., 2013; Fig. 1). However, the configuration of depth contours has a bend between the South Island and the Taranaki region for depths >75 km. Occasionally, small wiggles of the depth contours are related to the bicubic spline interpolation algorithm. A local change in the geometry of the subducting slab might lead to stress changes, with resultant variations in seismic signatures, particularly stress-sensitive seismic anisotropy. Thus, one of the objectives of this study is to characterize the slab deformation patterns at depth.

The Taupō Volcanic Zone (TVZ) – a NE-trending Quaternary volcanic arc and Mt. Taranaki are two striking geologic features at the central to western North Island. The TVZ has been attributed to backarc extension, which ceased in the Taranaki region in the Pliocene and then transferred

* Corresponding author at: Key Laboratory of Ocean and Marginal Sea Geology, South China Sea Institute of Oceanology, Chinese Academy of Sciences, China.
** Corresponding author.
E-mail addresses: cao_lingmin@126.com (L. Cao), xiaobo.he@zjou.edu.cn (X. He).

https://doi.org/10.1016/j.tecto.2024.230455
Received 30 May 2024; Received in revised form 25 July 2024; Accepted 3 August 2024
Available online 4 August 2024

northeastward (Stern et al., 2006; Giba et al., 2010). A recent study has emphasized the role of slab-derived fluids in high magma output rates at Ahi Tupua of the TVZ (Mark et al., 2024). Note that Mt. Taranaki is about 400 km west of the trench and 150 km west of the TVZ; explaing its existence within the context of the current subduction system needs more investigations (Fig. 1) (Reyners et al., 2007; Williams et al., 2013). Additionally, delamination of the lithosphere through thickening and convective removal has been postulated for the western North Island in the Taranaki region (Stern et al., 2006, 2013; Dimech et al., 2017). All geological and tectonic evidence suggests that the North Island of New Zealand has undergone an intricate tectonic history. This study aims to present the upper mantle dynamics in the backarc, which may not explicitly reveal the genesis of TVZ and Mt. Taranaki but is nevertheless crucial in comprehending how the upper mantle responds to the subduction of the Pacific plate.

Seismic anisotropy measurements from shear waves of teleseismic and deep local earthquakes shed light on the present-day mantle flow pattern and lithospheric deformation (Silver and Chan, 1991). Some previous anisotropy analyses focus on the eastern, southern, and central parts of the North Island (e.g., Gledhill and Stuart, 1996; Marson-Pidgeon et al., 1999; Marson-Pidgeon and Savage, 2004). One intriguing observation is that, except in the west and northwest of New Zealand, consistent fast-wave polarizations subparallel to the trench and delay times larger than 1.5 s (with the largest up to 4.5 s) were observed from core-refracted or teleseismic shear wave splitting measurements. The seismic anisotropy with trench-subparallel fast directions was interpreted to be caused by anisotropy in the mantle wedge, in the slab itself, and in the sub-slab mantle (e.g., Gledhill and Stuart, 1996; Marson-Pidgeon et al., 1999; Marson-Pidgeon and Savage, 2004; Audoine et al., 2004; Greve et al., 2008; Greve and Savage, 2009; Zal, 2020). These large delay times gave way abruptly to nearly zero delay times in the region west of the TVZ and north of 37.5° S latitude (Greve et al., 2008; Greve and Savage, 2009; Zal, 2020). Additionally, several studies carried out shear wave splitting of direct *S* waves from local shallow to intermediate subduction events (Brisbourne et al., 1999; Matcham et al., 2000; Audoine et al., 2000, 2004; Gerst and Savage, 2004; Morley et al., 2006; Johnson et al., 2011; Illsley-Kemp et al., 2019; Cao et al., 2023), targeting the local anisotropy structure above the subducting slab. These fast polarization directions vary considerably from place to place. Little shear wave splitting work has focused on the deep backarc of southwestern North Island (Taranaki and its adjacent regions). In this study, we examine data from a dense network of three-component broadband seismographs operated in Taranaki and investigate the spatial variation in seismic anisotropic parameters using teleseismic *SKS/S* waves and *S* waves from deep (> 150 km depth) local earthquakes.

2. Data and method

We collected local *S* and teleseismic *S/SKS* waveforms generated by events between December 2001 and September 2002, recorded by 41 three-component, broadband seismographs that belong to the Taranaki Volcano-Seismic Network (TVSN; Sherburn and White, 2005; Fig. 1 and

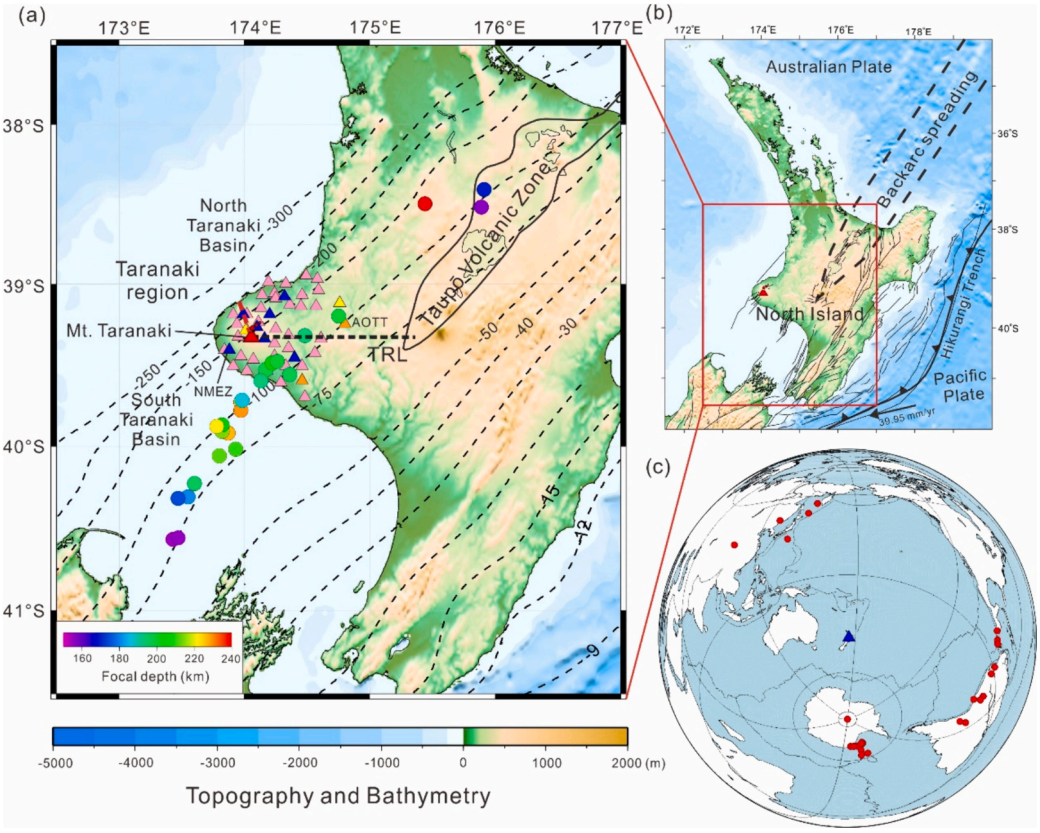

Fig. 1. Regional tectonic setting and distribution of events (circles) and stations (triangles) used in this study. (a) Topographic map showing the distribution of 43 TVSN broadband seismic stations (pink triangles), two Geonet long-term broadband seismic stations (yellow triangles), and seven Geonet long-term short-period seismic stations (blue triangles). The two stations (NMEZ and AOTT) used as examples showing splitting measurements in Fig. S1 are marked. Local events used in the final analysis are shown as circles, colored according to the depth ranging from 150 to 250 km. Dashed contours of the Pacific plate interface (in km) are from Williams et al. (2013). Dashed red line denotes the Taranaki Volcanic lineament. The Taranaki-Ruapehu Line (TRL) is marked by the dashed black line. (b) Regional tectonic setting of North Island of New Zealand. The black arrow shows the convergence rate between the Pacific and Australian plates (DeMets et al., 2010). The red rectangle shows the location of the study area. (c) Red circles show Mw > 6.0 teleseismic events with epicentral distances ranging from 60° to 135° used in the final analysis. The blue triangle shows the location of the central station in the study area. (For interpretation of the references to color in this figure legend, the reader is referred to the web version of this article.)

Table S1). We also collected local *S* and teleseismic *SKS* waveforms from 10-years (2012−2022) of recordings from two long-operating broadband seismic stations (KHET and VRT) and local *S* waveforms from seven short-period seismic stations (DREZ, LREZ, MHEZ, NEZ, NMEZ, PKE, PREZ) operated by GeoNet Aotearoa New Zealand (http://www.geonet.org.nz).

The event information for all local earthquakes was obtained from GeoNet (http://www.geonet.org.nz). For the teleseismic earthquakes we used the earthquake catalog from the US Geological Survey (USGS). For splitting measurements from local *S* phases, we examined seismograms generated by events (Mb >3.5) at depths of 150–600 km recorded at stations within a 35° cone (i.e., the so-called "shear wave window"; Booth and Crampin, 1985), calculated with the approximation of a straight-line propagation path. We limited our measurements to events with <5 km depth error and 2 km epicentral location error to reduce bias in anisotropy measurements due to ray path differences caused by the event location error. A total of 68 (2001/12/01–2002/9/9) and 118 (2012–2022) local earthquakes were used for the TVSN and GeoNet stations, respectively. We also selected earthquakes with epicentral distances from 85° to 135° for *SKS* recorded at the TVSN stations (19 earthquakes) and two GeoNet broadband seismometers (289 earthquakes). To complement teleseismic *SKS* splitting measurements for the TVSN stations, two more earthquakes with epicentral distances ranging from 60° to 80° and depths >420 km for teleseismic *S* for the TVSN stations were also chosen.

When shear waves propagate through an anisotropic region, they split into fast and slow propagating waves with perpendicular polarization directions (e.g., Nur and Simmons, 1969). The polarization of the fast wave, referred to as the fast direction (φ), reflects the orientation of seismic anisotropy in the region. The delay time between the fast and slow waves (δt) provides constraints on the strength of anisotropy and/or the thickness of the anisotropic layer (e.g., Hess, 1964; Silver, 1996; Savage, 1999; Long and Silver, 2009; Liu and Gao, 2013; Long and Lynner, 2015). Ray paths from teleseismic and deep earthquakes usually are longer in the mantle than in the crust, but if they are recorded at the surface, all parts of the path must be considered. To constrain the relative contribution of mantle flow above, within and below the subducting slab, splitting measurements from multiple phases, such as local *S*, source-side *S,* and teleseismic *SKS* waves, can be combined to consider the source of observed anisotropy (Long, 2013; Long and Wirth, 2013). In this study, we combined local *S*, teleseismic *S,* and *SKS* splitting to discuss the source of observed anisotropy in the following sections.

Following data processing procedures described in the previous studies by Brisbourne et al. (1999), Audoine et al. (2004) and Greve et al. (2008), who carefully tested the filters based on the noisy nature in New Zealand stations, we band-pass filtered the original broadband waveforms at 0.5–3 Hz for the local *S* phases and 0.01–0.1 Hz for the teleseismic *SKS* and *S waves*, respectively, to enhance the signal to noise ratio of the shear wave arrivals. We employed the Multiple Frequency Automatic Splitting Technique (MFAST) program (Teanby et al., 2004; Savage et al., 2010; Wessel, 2010) on the local and teleseismic *S* waves to constrain the seismic anisotropic parameters φ and δt because it is particularly suitable when the initial polarization of the *S* wave is unknown. The MFAST and the SplitLab toolkit (Wüstefeld et al., 2008) were used to analyze the *SKS* wave splitting. We considered two different delay time ranges: from 0.01 to 1.5 s and from 0.01 to 0.4 s for local earthquakes. For 1.5 s time windows, the results were either consistent with the 0.4 s time windows, or unstable, so we used the second delay time range for the final measurements. We used delay times ranging from 0.01 to 6.0 s for teleseismic SKS waveforms. In general, the results are considered to be well constrained if they have the following characteristics after splitting correction: (1) good correlation between the fast and slow waveforms, (2) insignificant amplitude on the perpendicular component of incoming polarization direction for local/teleseismic *S* waves or on the transverse component of *SKS* waves, (3) good linearization of particle motion, and (4) small 95% confidence regions (Silver and Chan, 1991; Savage et al., 2010; Wessel, 2010). Figs. S1 and S2 show representative examples of local *S* and teleseismic *S* wave splitting measurements from MFAST and all *SKS*-wave splitting from SplitLab. A null result occurs when the shear wave travels in an isotropic medium or the initial polarization of *S* phase (or *SKS* back-azimuth) aligns with the fast or slow polarization direction (e.g., Silver and Chan, 1991; Wüstefeld and Bokelmann, 2007); this information can place additional constraints on the nonnull splitting measurements (e.g., Silver and Chan, 1991; Cao et al., 2021), which are presented them in Fig. S3.

SplitLab provides three different methods: the rotation correlation method (RC; Bowman and Ando, 1987), the minimum energy method (SC; Silver and Chan, 1991), and the eigenvalue method (EV; Silver and Chan, 1991). In contrast, MFAST exclusively uses the EV method. Previous studies by Wüstefeld and Bokelmann (2007) and Vecsey et al. (2008) have highlighted that both RC and SC methods can yield poor results near null directions, while the SC method generally provides stable estimates across a broad range of back-azimuths, except at null directions. The RC often requires waveforms with a high signal-to-noise ratio to perform well. That is to say, SC performs better than RC under various conditions. Seven out of thirteen *SKS* splitting measurements showed aless than 10° difference in fast direction between RC and SC, while the remaining six did not. Given the greater stability of SC, we used splitting parameters from SC in the final analysis.

3. Results

Based on the selection criterion vriteria, our analysis produced 34 local *S* splitting measurements from 24 local events recorded at 18 stations, 24 high-quality teleseismic *SKS* and *S*-wave splitting measurements from 10 teleseismic events recorded at 16 stations, and 28 null results for teleseismic *SKS* and *S* waves from 24 events (Tables S2–S6; Figs. 2 and 3).

Overall, the local *S* delay times (average 0.17 ± 0.01 s) are small, with values <0.4 s, which largely exceed the resolution of measurements on the order of 0.01 s; the fast polarization varies from trench-parallel (53.8 ± 0.74°) in the northeast to trench-oblique (22 ± 6.54°) in the center, and finally to trench-normal (−63.77 ± 7.49°) in the southwest.

The delay times of *SKS* phases, averaging 2.70 ± 0.24 s, vary from 1.78 to 3.65 s, and the fast polarizations consistently exhibit trench-parallel orientation. Results with larger delay times (>2.80 s) are predominantly (>67%) clustered offshore (see Area B in Fig. 3a) according to the distribution of the pierce points of *SKS* ray paths at a depth of 200 km. Six teleseismic *S* and 25 *SKS* waves yield null measurements, with incoming polarizations for *S* and back-azimuths for *SKS* either normal or parallel to the dominant fast directions (Fig. 3a and Table S6).

4. Discussion

4.1. Anisotropic sources for local S splitting

Local *S*-splitting results from deep earthquakes with paths in the northeast (Fig. 2) show a trench-parallel fast-polarization pattern (NE–SW). This pattern is broadly consistent with the crustal anisotropy pattern from shallow earthquakes observed on the flanks of Mt. Taranaki, which are also predominantly align NE–SW (Fig. 4 in Illsley-Kemp et al., 2019). However, they are notably different from the NW–SE alignment seen from shallow local earthquakes recorded by stations near the Taranaki Volcanic Lineament shown in Fig. 1a (Illsley-Kemp et al., 2019). To characterize shallow upper mantle deformation, Cao et al. (2023) analyzed the local data from the events between 70 and 150 km depths and obtained the NNE–SSW alignment (Fig. 2). Specifically, the fast directions in the northeast from Cao et al. (2023) with an average of 13.5 ± 1.76° deviate by ~22° from the convergence direction of 261° between the Australian and Pacific plates (DeMets et al., 2010; Fig. 2). Although Audoine et al. (2004) reported many trench-normal

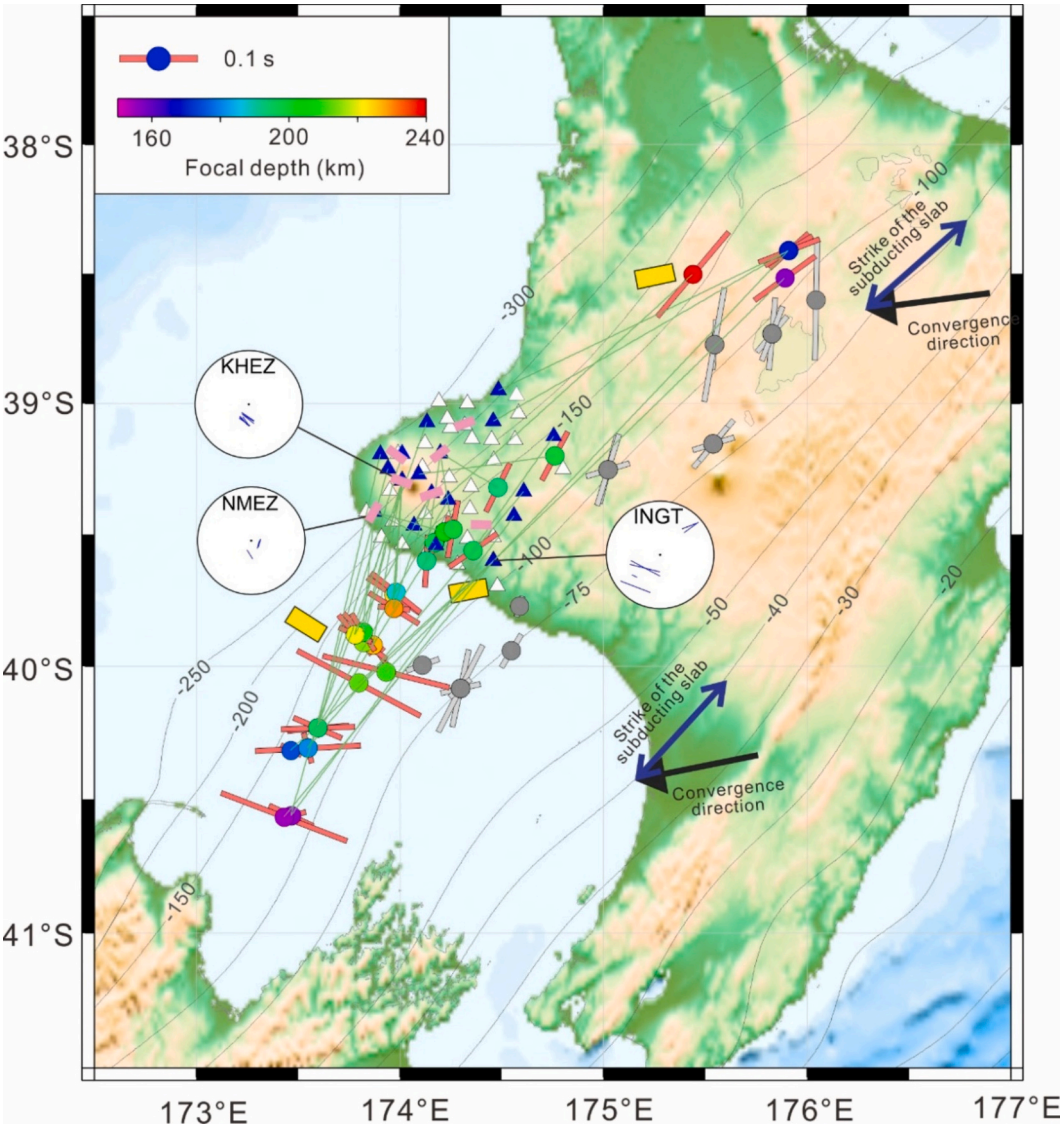

Fig. 2. Local *S*-phase splitting measurement results showing the distribution of events (circles) and stations (triangles), with blue stations yield final reliable splitting measurements. The fast polarizations are plotted at the epicenters of the events (circles colored according to the focal depth). The orientation of each bar is parallel to measured fast polarization; length is scaled according to delay time. Ray paths between events and stations are shown with green lines. The three circular diagrams show the lower hemisphere, equal-area projections of the splitting parameters at each station, with the outer circle represents an incidence angle of 40°. Pink bars represent the predominant fast directions of the crustal seismic anisotropy in the Taranaki region from Illsley-Kemp et al. (2019). Grey bars indicate the local S-wave splitting measurements from events with depth between 70 and 150 km as measured by Cao et al. (2023). Yellow thick bars denote maximum horizontal compressive stress (SHmax) orientations inferred from focal mechanisms, revealing the orientation of the stress field at the neighboring slab contour depths (Townend et al., 2012). (For interpretation of the references to color in this figure legend, the reader is referred to the web version of this article.)

fast directions from shallow to deep-focus events beneath the TVZ extensional region, more recent work with a more extensive network and longer time frame (Illsley-Kemp et al., 2019) yields more complex anisotropic results. These include trench-parallel fast directions in general disrupted by variable measurements from shallow earthquakes under calderas.

Our results indicate the presence of a depth-independent anisotropy in the upper mantle with NE–SW fast directions (Fig. S4). Due to the limited vertical resolution of shear-wave splitting, it is challenging to constrain the contribution from each anisotropic layer, mainly because of the nonlinear effects of overlapping anisotropic layers (e.g., Silver and Savage, 1994; Rümpker and Silver, 1998). In the northeast of the Taranaki region and within the TVZ, the trench-parallel anisotropy in the crust observed by Illsley-Kemp et al. (2019) for earthquakes <40 km depth can be attributed to the alignment of fluid-filled fractures (Crampin, 1987) parallel to the direction of maximum compressive stress measured by Townend et al. (2012). Nearby events with 70–150 km depths show fast polarizations at ~30° (i.e., NNE–SSW), whereas the shallow crustal events primarily exhibit NE-SW fast polarizations (Illsley-Kemp et al., 2019; Cao et al., 2023). Importantly, the delay times do not vary with depth (Fig. S4), which suggests that the shallowest crustal anisotropic layer, which is related to the local maximum compressive stress, has the most significant effect on the shear-wave splitting measurement (Rümpker and Silver, 1998).

Although delay times exhibit depth-independent variations between 150 and 250 km in this study (Fig. S4), the ray paths from events primarily sample the shallow part of the subducting slab. Another possible explanation for the trench-parallel fractures is the bending of the incoming oceanic plate as it approaches the subduction zone (Fig. 4). This outer-rise bending induces significant extensional stresses, forming fractures oriented parallel to the trench axis. Such fractures have been confirmed through observations (e.g., Wang et al., 2022; Liu et al., 2022;

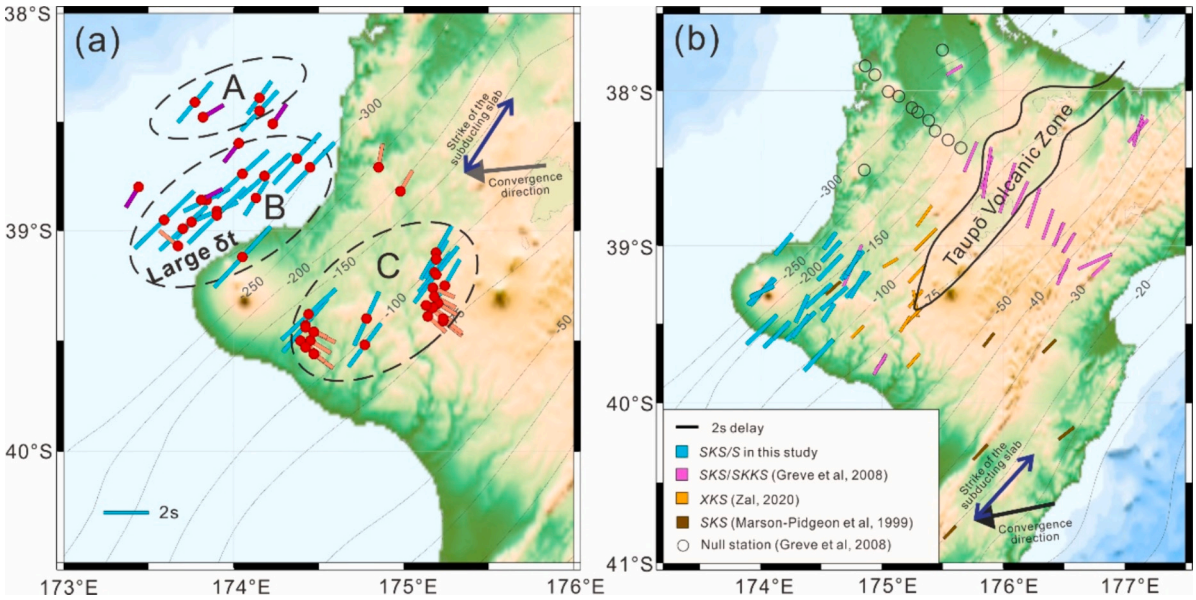

Fig. 3. (a) Results of all teleseismic *SKS*-wave and *S*-wave splitting measurements from this study, plotted at the 200 km depth pierce points (red circles) of the ray paths. The orientation of each blue bar indicates the corresponding fast direction; the bar length is proportional to the delay time. Orange and purple bars represent null measurements, showing back-azimuth and incoming polarization directions for *SKS* (orange) and *S* waves, respectively. (b) Comparison of teleseismic *SKS/S*-wave splitting observations from this study and previous splitting (Greve et al., 2008; Marson-Pidgeon and Savage, 2004; Zal, 2020). Results are plotted at the locations of stations. (For interpretation of the references to color in this figure legend, the reader is referred to the web version of this article.)

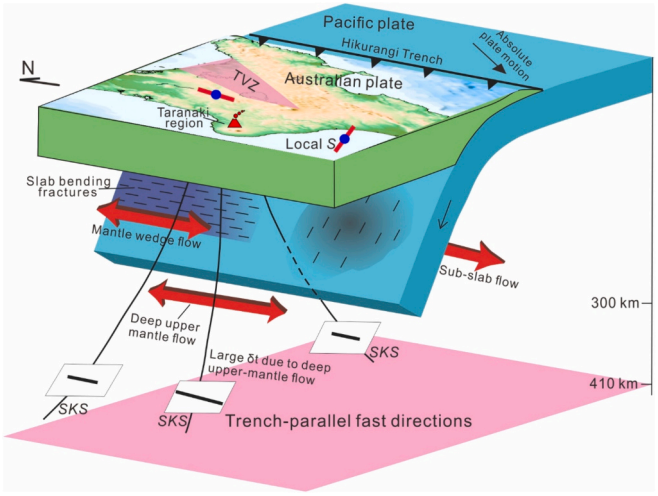

Fig. 4. Schematic cartoon illustrating the major tectonic setting of the Hikurangi subduction zone and the interpreted mantle flows. On the surface, the orientations of the two solid red bars indicate the predominant fast polarization directions from local *S* wave splitting in the northeast and southwest, respectively. The representative *SKS/S*-wave ray paths in the upper mantle are marked with curved black lines. (For interpretation of the references to color in this figure legend, the reader is referred to the web version of this article.)

Lynner et al., 2024) and numerical modeling (Faccenda et al., 2008) in other regions. Eberhart-Phillips and Reyners (2009) also found that *P*-wave speed within the slab in this region is fast in the trench-parallel orientation. However, given that paths through such a small section of the slab are unlikely long enough to accrue substantial splitting, so modeling or some other technique is needed to confirm this hypothesis.

B-type olivine crystallographic preferred orientation (CPO) has occasionally been used to explain trench-parallel mantle wedge anisotropy when corner flow dominates in the wedge (e.g., Katayama and Karato, 2006). However, if B-type olivine exists, it is more likely to occur in the forearc wedge because it can be extensively hydrated (Hyndman and Peacock, 2003). Recent studies suggested that the forearc wedge is mainly isotropic because of its stagnant nature, in which it does not participate in the mantle wedge flow (Uchida et al., 2020). In contrast, the backarc region is less likely to contain B-type olivine (Katayama and Karato, 2006). Since this study focuses on the backarc, so B-type olivine is less likely to explain the trench-parallel anisotropy. Thus, the local event signals are likely due to crustal fractures caused by the regional maximum compressive stress, with possible additional signals coming from fractures due to the outer-rise bending of the incoming plate.

The trench-normal anisotropy observed from local earthquakes in the southwest (Fig. 2) is intriguing as it contrasts to most other measurements and is only observed in this region. Previous local *S*-wave splitting studies reported NE–SW or E–W-trending fast directions in the Taranaki crust (Illsley-Kemp et al., 2019), consistent with the region's compressive stress (Townend et al., 2012), and trench-parallel (NE–SW) fast directions in the shallow upper mantle between 70 and 150 km depth beneath the South Taranaki basin (Cao et al., 2023). Although most previous *SKS/S* splitting measurements in the southern North Island yield trench-parallel fast polarizations (Fig. 3b; Marson-Pidgeon et al., 1999; Audoine et al., 2004; Greve et al., 2008; Eberhart-Phillips and Reyners, 2009; Zal, 2020), none of them have been recorded for paths traversing this region. Therefore, we speculate that such a trench-normal signature can be caused by delamination near the Taranaki-Ruapehu line (Stern et al., 2013; Dimech et al., 2017) and/or compressive stress in the slab (Townend et al., 2012). The evidence for regional delamination includes a thin crust and lithosphere north of the TRL and low *P* and *S* wave velocities in the upper mantle (Horspool et al., 2006; Salmon et al., 2011; Seward et al., 2009). These findings suggest that the destruction of the mantle lithosphere occurred in the TVZ and west of it. The destruction process may be accompanied by small-scale convection in the upper mantle, leading to little anisotropy. Trench-normal anisotropy may develop due to the dynamic interaction between delamination and slab subduction, which requires further numerical modeling verification. A similar delamination phenomenon has been proposed in Hokkaido, Japan (Koulakov et al., 2015). The authors suggested that the delaminated material prevents the escape of fluids and melts upwards. In our study area, the mantle wedge flow above the subducting slab orients trench-parallel, which will be discussed in

Section 4.2. Given that delay times from local earthquakes in the southwest do not vary with depths from 70 to 250 km, as shown by this study and previous measurements (Cao et al., 2023; Fig. S4), we suggest that the trench-normal fast directions are likely related to the deflected mantle flow caused by prevention of delaminated material which might sink to 80 km depth according to seismic tomographic images (Dimech et al., 2017).

Another scenario that may explain the trench-normal fast directions in the southwest is related to the strain in the subducting slab. Townend et al. (2012) inverted the focal mechanisms of intraslab earthquakes to derive the intraslab stress field. Their results suggested the compressive stress in the slab beneath the South Taranaki basin, which aligns with our observations here (Fig. 4).

4.2. Anisotropic sources for SKS splitting

Before explaining the anisotropic source of *SKS* splitting, we discuss the olivine fabrics that could contribute to the observations. C- and E-type fabrics can produce different splitting results at large incidence angles ($> 30°$). According to previous studies (e.g., Karato et al., 2008), stress, water content and pressure conditions control the type of olive fabric. A-type fabrics dominate the lithosphere, C-type fabrics form under deep, water-rich environments, and C- and E-type fabrics form in the asthenosphere in the mantle wedge. Since the incidence for all *SKS* waves in this study is $<10°$, and the fast axis for both C- and E-type aligns with the flow direction, neither fabric types nor incidence angles will affect our interpretations.

In this study, the most prominent signature of seismic anisotropy from *SKS* splitting (Fig. 3) is the trench-parallel fast-polarization pattern, which is consistent with the predictions of our null measurements. This observation suggests a regionally coherent mantle deformation, extending the previously determined NE/SW fast polarization orientations to the Taranaki region in the west. As noted earlier, there is a limited vertical resolution in shear-wave splitting. The contributions to *SKS* splitting may come from the overriding crust, mantle wedge, downgoing slab, and sub-slab flow. Many local S splitting measurements are nearly parallel to those from the *SKS* phases, suggesting either similar fast directions at several depths, or rotation of fast directions as they approach the surface (e.g., Rümpker and Silver, 1998). Although local earthquakes' fast directions vary rapidly with location and *SKS* waves' fast directions are coherent across a broad region, the *SKS* waves are likely not affected much by the overriding crustal anisotropy.

Three areas are defined based on the distribution of *SKS*-wave ray piercing points at the 200 km depth for this study (Areas A, B and C in Fig. 3a). Specifically, in the northwest and center regions (offshore Taranaki, Areas A and B) the *SKS*-waves primarily sample the overriding crust and the mantle wedge. In contrast, in the southeast (Area C), the *SKS*-waves predominantly sample the crust, the mantle wedge, the subducting lithosphere and the sub-slab mantle (Fig. 4). As noted earlier, the contribution from the overriding crust to shear wave splitting can be considered negligible.

In Area C, trench-parallel anisotropy may be caused by trench-parallel flow both above and below the slab, as well as trench-parallel anisotropy within the slab, as suggested by previous regional studies (e.g., Marson-Pidgeon and Savage, 2004). Although trench-parallel slab fabrics have been proposed to explain some trench-parallel anisotropy (Audoine et al., 2000; Brisbourne et al., 1999; Gledhill and Stuart, 1996; Matcham et al., 2000), their contribution to teleseismic splitting may not be significant due to the limited paths sampling the slab. Therefore, we attribute the trench-parallel anisotropy mainly to flow above and below the slab. Unfortunately, the relative importance of flow above and below the slab is hard to precisely distinguish due to the poor depth resolution of teleseismic splitting. Based on the recordings of intermediate-depth events, local shear-wave splitting, reflecting the anisotropy above the slab, mainly yields small delay times (0.1–0.3 s). They are notably smaller than teleseismic measurements (>2 s). Therefore, sub-slab flow is likely dominant in explaining the trench-parallel anisotropy.

Two global models, Walpole et al. (2017) and Lynner and Long (2014), suggest that widespread trench-parallel anisotropy may result from slab rollback due to slab-asthenosphere decoupling (Russo and Silver, 1994). However, the underlying mechanism for this decoupling remains unclear. A recent study proposed that a weak layer along the slab-asthenosphere interface in the deep upper mantle could form due to grain-size-sensitive creep of olivine induced by oxidation of olivine, thereby facilitating trench-parallel flow above and below the subducting slab (Ohuchi, 2022), which supports our observations related to trench-parallel mantle flow in Area C.

The average δt at stations in the furthest northwest (Area A) and the furthest southeast (Area C) are 2.15 ± 0.27 s and 2.66 ± 0.41 s, respectively, while δt in the middle (Area B) has a larger average of 2.80 ± 0.62 s with the largest reaching up to 3.65 s (Fig. 3a). Larger δt up to 4.5 s from *SKS*-phase splitting analysis in the TVZ and central northern North Island of New Zealand has been attributed to aligned melt bands in the mantle wedge (Audoine et al., 2004; Greve et al., 2008). Nevertheless, this study cannot apply this mechanism to Area B because we found smaller delay times (0.1–0.3 s) from local *S* splitting from earthquakes up to ~200 km deep, showing no evidence of significant melts in the mantle wedge mentioned above. In Area B, we attribute the trench-parallel fast directions to edge effects due to its proximity to the southern edge of the subducting Pacific slab. Similar trench-parallel flows have been observed in other subduction zones, such as the Sumatra and Alaska-Aleutian subduction zones (Kong et al., 2020; Lynner et al., 2024). However, the large δt in Area B could result from a deep upper-mantle (200–400 km depth) deformation, or it may be related to the delamination proposed by Dimech et al. (2017). In Area A, δt is not very large, likely because it is distant from the area influenced by deep interaction and delamination.

Deep upper-mantle anisotropy in this region is evidenced by the global surface wave anisotropic model by Debayle et al. (2016) (Fig. S5) despite limited lateral resolution. Our *SKS* splitting observations are consistent with deep upper-mantle flow. More specifically, given a coherent deformation above the 410 km discontinuity, we assume that the crust and shallow upper mantle of ~200 km thickness with 2% anisotropy may result in a splitting time of 1 s (Silver, 1996). The deep upper mantle would need to contribute 2–2.5 s of splitting, corresponding to ~5.3–6.7% anisotropy for a 150-km thick anisotropic layer based on experimental data for mantle-derived xenoliths (e.g., Mainprice and Silver, 1993; Ismaïl and Mainprice, 1998). Yuan and Romanowicz (2010) used azimuthal anisotropy tomography to find 2% anisotropy from 200 to 400 km deep in the northwestern US. Vigorous mantle flow, the presence of hydrous minerals in the upper mantle (Karato et al., 2008), and the shape-preferred orientation of partial melt (Long et al., 2009) have been proposed as the main reasons for the anomalously large shear-wave splitting times observed. Beneath the Cascadia backarc, the anisotropy source of the large delay times can be constrained to the deep upper mantle (Mondal and Long, 2020). The trench-normal fast directions in the deep upper mantle of the Cascadia subduction zone are different from the trench-parallel directions in the Hikurangi subduction zone; the difference can be caused by different dynamic processes atop the 410 km discontinuity. Notably, shear wave splitting measurements in the Cascadia subduction zone (Mondal and Long, 2020) show that the interaction between the subducting slab and the 410 km discontinuity can enhance the anisotropy strength of the deep upper mantle. This is likely the case at Taranaki where the subducting slab (seismic portion) in this region has reached a depth of >300 km (Williams et al., 2013) and the aseismic segment may have contacted the 410-km depth discontinuity. The interaction between the downwelling and the 410 km discontinuity may cause intense deformation, leading to strong anisotropy in the deep upper mantle (that is, the 410 discontinuity acts as a barrier against the downwelling) (Fig. 4). The specific interactions between the subducting slab and the 410 km discontinuity and the detailed mechanisms by which this process leads

to changes in the strength of upper mantle anisotropy require further validation from continued in-depth research.

4.3. Inferred regional upper-mantle dynamics

In the central northern North Island, the TVZ is a volcanic arc aligned with the axis of backarc extension. Regional dynamics may be controlled by trench-parallel flow both above and below the slab (Fig. 4), attributed to backarc extension due to the rollback of the Pacific plate and rotation of the overlying Australian plate. There is no apparent 2-D corner flow prevails in the mantle wedge beneath the TVZ and Taranaki. However, 2-D corner flow might explain the local shear-wave splitting for events between Taranaki and the South Island. The absence of corner flow may be related to the inactive arc volcanoes in this region and to the general compression south of the TVZ, as previously suggested (e.g., Audoine et al., 2004; Stern et al., 2006). The reason for this is that corner flow plays a crucial role in dragging the partially serpentinized forearc mantle down into the sub-arc depths and the entrained forearc mantle fragments are further metasomatized by slab fluids/melts derived from the dehydration of serpentinites in the downgoing slab (Li et al., 2021).

In contrast, extension promotes magma to rise from deep in this intra-arc rift environment (Gase et al., 2019). Extension rates decrease southward to 5 mm/yr at the southern end of the TVZ and turn compressive south of the TVZ (Walcott, 1984; Wallace et al., 2004). Consequently, the absence of corner flow and compression in the southern North Island may result in insufficient fluids and melts in the sub-arc mantle (that is, those in the forearc avoid being transported), thereby forming a volcanic arc quiescence in this region.

5. Conclusions

We characterized upper-mantle anisotropy in the backarc Taranaki region of the Hikurangi subduction zone by analyzing teleseismic *SKS, S waves,* and local *S* waves. Our analyses provide insights inon upper-mantle flow patterns and anisotropic structure in the Taranaki region in previously unexplored areas offshore to the west and south of Taranaki. The key observations and interpretations are as follows.

1. Fast polarizations from deep local *S* waves vary markedly from trench-parallel in the northeast to trench-normal in the southwest. In contrast, those for teleseismic waves consistently show trench-parallel. In this study, the teleseismic shear waves measured traverse the northwest and east regions but do not intersect the southwest area, where local S waves display seismic anisotropy perpendicular to the trench.
2. The trench-parallel anisotropy for teleseismic waves may result from trench-parallel flow above or below the slab or by a highly anisotropic slab itself. Dynamic interaction between the subducting slab and the 410 km discontinuity could account for a region with large delay times.
3. The trench-parallel anisotropy for local *S*-waves may result from regional stress or by fractures induced by outer-rise bending in the down-going slab. In contrast, the trench-normal anisotropy for local *S*-waves might be attributed to local stresses in the subducting slab or near the seismic stations.

CRediT authorship contribution statement

Lingmin Cao: Writing – review & editing, Writing – original draft, Visualization, Methodology, Data curation, Conceptualization. **Xiaobo He:** Writing – review & editing, Supervision, Formal analysis. **Huaiyu Yuan:** Writing – review & editing, Supervision. **Minghui Zhao:** Validation, Formal analysis, Conceptualization. **Xuelin Qiu:** Writing – review & editing, Validation, Conceptualization. **Martha K. Savage:** Writing – review & editing, Validation, Formal analysis.

Declaration of competing interest

The authors declare that they have no known competing financial interests or personal relationships that could have appeared to influence the work reported in this paper.

Data availability

All individual measurements and the summary file in this study can be accessed from https://zenodo.org/record/7579375.

Acknowledgments

We want to express our sincere gratitude to Kelly Liu and Ian Bastow for their insightful comments and suggestions, which have significantly improved the quality of this manuscript. We appreciate the New Zealand GeoNet project and its sponsors EQC, GNS Science, LINZ, NEMA and MBIE, and the Data Management Center of the Incorporated Research Institutions for Seismology (www.iris.edu) and GeoNet (https://www.geonet.org.nz) for providing all seismic data used in this study. We acknowledge support from the National Scientific Foundation of China (Grant Nos. 42076068 and 42488201), the Development Fund of South China Sea Institute of Oceanology of Chinese Academy of Sciences (No. SCSIO202207) and the Strategic Priority Research Program of the Chinese Academy of Sciences (Grant No. XDB42020103). The Multiple Frequency Automatic Splitting Technique software can be obtained via http://mfast-package.geo.vuw.ac.nz/. Some figures were prepared using the Generic Mapping Tools (P. Wessel & Smith, 1991).

Appendix A. Supplementary data

Supplementary data to this article can be found online at https://doi.org/10.1016/j.tecto.2024.230455.

References

Audoine, E., Savage, M.K., Gledhill, K., 2000. Seismic anisotropy from local earthquakes in the transition region from a subduction to a strike-slip plate boundary, New Zealand. J. Geophys. Res. Solid Earth 105 (B4), 8013–8033. https://doi.org/10.1029/1999JB900444.

Audoine, E., Savage, M.K., Gledhill, Ken, 2004. Anisotropic structure under a back arc spreading region, the Taupo Volcanic Zone, New Zealand. J. Geophys. Res. Solid Earth 109 (B11). https://doi.org/10.1029/2003JB002932.

Booth, D.C., Crampin, S., 1985. Shear-wave polarization on a curved wavefront at an isotropic free surface. Geophys. J. R. Astron. Soc. 83, 31–45.

Bowman, J.R., Ando, M., 1987. Shear-wave splitting in the upper-mantle wedge above the Tonga subduction zone. Geophys. J. R. Astron. Soc. 88, 25–41.

Brisbourne, A., Stuart, G., Kendall, J.-M., 1999. Anisotropic structure of the Hikurangi subduction zone, New Zealand—integrated interpretation of surface-wave and body-wave observations. Geophys. J. Int. 137 (1), 214–230. https://doi.org/10.1046/j.1365-246x.1999.00786.x.

Cao, L., He, X., Zhao, L., Lü, C., Hao, T., Zhao, M., Qiu, X., 2021. Mantle Flow patterns beneath the Junction of Multiple Subduction Systems between the Pacific and Tethys Domains, SE Asia: Constraints from SKS-Wave Splitting Measurements. Geochem. Geophys. Geosyst. 22 (9) https://doi.org/10.1029/2021gc009700.

Cao, L.M., Zhao, L., Zhao, M.H., Qiu, X.L., Yuan, H.Y., 2023. Anisotropic structure under the back arc region, Taranaki, New Zealand. J. Trop. Oceanogr. 42 (1), 124–134. http://www.jto.ac.cn/CN/10.11978/2022021 (Abstract in English).

Crampin, S., 1987. Geological and industrial implications of extensive-dilatancy anisotropy. Nature 328, 491–496.

Debayle, E., Dubuffet, F., Durand, S., 2016. An automatically updated *S*-wave model of the upper mantle and the depth extent of azimuthal anisotropy. Geophys. Res. Lett. 43, 674–682. https://doi.org/10.1002/2015GL067329.

DeMets, C., Gordon, R.G., Argus, D.F., 2010. Geologically current plate motions. Geophys. J. Int. 181 (1), 1–80.

Dimech, J.L., Stern, T., Lamb, S., 2017. Mantle earthquakes, crustal structure, and gravitational instability beneath western North Island, New Zealand. Geology 45 (2), 155–158.

Eberhart-Phillips, D., Reyners, M., 2009. Three-dimensional distribution of seismic anisotropy in the Hikurangi subduction zone beneath the central North Island, New Zealand. J. Geophys. Res. Solid Earth 114 (B6).

Faccenda, M., Burlini, L., Gerya, T.V., Mainprice, D., 2008. Fault-induced seismic anisotropy by hydration in subducting oceanic plates. Nature 455 (7216), 1097–1100. https://doi.org/10.1038/nature07376.

Gase, A.C., Van Avendonk, H.J.A., Bangs, N.L., Luckie, T.W., Barker, D.H.N., Henrys, S. A., Bassett, D., Okaya, D.A., Jacobs, K.M., Kodaira, S., Fujie, G., Arnulf, A.F., Yamamoto, Y., 2019. Seismic evidence of magmatic rifting in the offshore Taupo Volcanic Zone, New Zealand. Geophys. Res. Lett. 46, 12,949–12,957. https://doi.org/10.1029/2019GL085269.

Gerst, A., Savage, M.K., 2004. Seismic anisotropy beneath Ruapehu volcano: a possible eruption forecasting tool. Science 306 (5701), 1543–1547.

Giba, M., Nicol, A., Walsh, J.J., 2010. Evolution of faulting and volcanism in a back-arc basin and its implications for subduction processes. Tectonics 29. https://doi.org/10.1029/2009TC002634. TC4020.

Gledhill, K., Stuart, G., 1996. Seismic anisotropy in the fore-arc region of the Hikurangi subduction zone, New Zealand. Phys. Earth Planet. Inter. 95 (3), 211–225. https://doi.org/10.1016/0031-9201(95)03117-0.

Greve, S.M., Savage, M.K., 2009. Modelling seismic anisotropy variations across the Hikurangi subduction margin, New Zealand. Earth Planet. Sci. Lett. 285 (1–2), 16–26.

Greve, S.M., Savage, M.K., Hofmann, S.D., 2008. Strong variations in seismic anisotropy across the Hikurangi subduction zone, North Island, New Zealand. Tectonophysics 462 (1), 7–21.

Hess, H., 1964. Seismic anisotropy of the uppermost mantle under Oceans. Nature 203, 629–631. https://doi.org/10.1038/203629a0.

Horspool, N., Savage, M.K., Bannister, S., 2006. Implications for intraplate volcanism and backarc deformation in northwestern New Zealand from joint inversion of receiver functions and surface waves. Geophys. J. Int. 166, 1466–1483. https://doi.org/10.1111/j.1365-246X.2006.03016.x.

Hyndman, R.D., Peacock, S.M., 2003. Serpentinization of the forearc mantle. Earth Planet. Sci. Lett. 212 (3–4), 417–432.

Illsley-Kemp, F., Savage, M.K., Wilson, C.J.N., Bannister, S., 2019. Mapping stress and Structure from Subducting Slab to Magmatic Rift: Crustal Seismic Anisotropy of the North Island, New Zealand. Geochem. Geophys. Geosyst. 20 (11), 5038–5056. https://doi.org/10.1029/2019GC008529.

Ismaïl, W.B., Mainprice, D., 1998. A statistical view of the strength of seismic anisotropy in the upper mantle based on petrofabric studies of ophiolite and xenolith samples. Tectonophysics 296, 145–157.

Johnson, J.H., Savage, M.K., Townend, J., 2011. Distinguishing between stress-induced and structural anisotropy at Mount Ruapehu Volcano, New Zealand. J. Geophys. Res. Solid Earth 116 (B12).

Karato, S.-I., Jung, H., Katayama, I., Skemer, P., 2008. Geodynamic significance of seismic anisotropy of the upper mantle: New insights from laboratory studies. Annu. Rev. Earth Planet. Sci. 36 (1), 59–95.

Katayama, I., Karato, S.I., 2006. Effect of temperature on the B-to C-type olivine fabric transition and implication for flow pattern in subduction zones. Phys. Earth Planet. Inter. 157 (1–2), 33–45.

Kong, F., Gao, S.S., Liu, K.H., Zhang, J., Li, J., 2020. Seismic anisotropy and mantle flow in the Sumatra subduction zone constrained by shear wave splitting and receiver function analyses. Geochem. Geophys. Geosyst. 21 https://doi.org/10.1029/2019GC008766 e2019GC008766.

Koulakov, I., Kukarina, E., Fathi, I.H., El Khrepy, S., Al-Arifi, N., 2015. Anisotropic tomography of Hokkaido reveals delamination-induced flow above a subducting slab. J. Geophys. Res. Solid Earth 120, 3219–3239. https://doi.org/10.1002/2014JB011823.

Li, H.-Y., Zhao, R.-P., Li, J., Tamura, Y., Spencer, C., Stern, R.J., Ryan, J.G., Xu, Y.G., 2021. Molybdenum isotopes unmask slab dehydration and melting beneath the Mariana arc. Nat. Commun. 12 (1), 6015. https://doi.org/10.1038/s41467-021-26322-8.

Liu, K.H., Gao, S.S., 2013. Making reliable shear-wave splitting measurements. Bull. Seismol. Soc. Am. 103 (5), 2680–2693. https://doi.org/10.1785/0120120355.

Liu, Y., Xue, M., Guo, Z., Zhu, A., 2022. Seismic anisotropy within the subducting northern Philippine Sea plate, SW Japan, using DONET seafloor observation network. Geophys. Res. Lett. 49 https://doi.org/10.1029/2021GL096516.

Long, M.D., 2013. Constraints on subduction geodynamics from seismic anisotropy. Rev. Geophys. 51 (1), 76–112. https://doi.org/10.1002/rog.20008.

Long, M.D., Lynner, C., 2015. Seismic anisotropy in the lowermost mantle near the Perm Anomaly. Geophys. Res. Lett. 42, 7073–7080. https://doi.org/10.1002/2015GL065506.

Long, M.D., Silver, P.G., 2009. Shear wave splitting anisotropy: Measurements, interpretation, and new directions. Surv. Geophys. 30, 407–461.

Long, M.D., Wirth, E.A., 2013. Mantle flow in subduction systems: the mantle wedge flow field and implications for wedge processes. J. Geophys. Res. Solid Earth 118 (2), 583–606.

Long, M.D., Gao, H., Klaus, A., Wagner, L.S., Fouch, M.J., James, D.E., Humphreys, E., 2009. Shear wave splitting and the pattern of mantle flow beneath eastern Oregon. Earth Planet. Sci. Lett. 288, 359–369.

Lynner, C., Long, M.D., 2014. Sub-slab anisotropy beneath the Sumatra and circum-Pacific subduction zones from source-side shear wave splitting observations. Geochem. Geophys. Geosyst. 15 (6), 2262–2281.

Lynner, C., Toro-Acosta, C., Paulson, E., Birkey, A., 2024. Local-S shear wave splitting along the length of the Alaska–Aleutian subduction zone. Geophys. J. Int. 237 (3), 1567–1574.

Mainprice, D., Silver, P.G., 1993. Interpretation of SKS waves using samples from the subcontinental lithosphere. Phys. Earth Planet. Inter. 78, 257–280.

Mark, O.K., Illsley-Kemp, F., Townend, J., Barker, S.J., 2024. Evidence from Intermediate-Depth Earthquakes of Slab-Derived Fluids beneath the Taupō Volcanic Zone. J. Geophys. Res. Solid Earth 129 (5). https://doi.org/10.1029/2023jb028586.

Marson-Pidgeon, K., Savage, M.K., 2004. Shear-wave splitting variations across an array in the southern North Island, New Zealand. Geophys. Res. Lett. 31 (21) https://doi.org/10.1029/2004gl021190.

Marson-Pidgeon, K., Savage, M.K., Gledhill, K., Stuart, G., 1999. Seismic anisotropy beneath the lower half of the North Island, New Zealand. J. Geophys. Res. Solid Earth 104 (B9), 20277–20286. https://doi.org/10.1029/1999JB900212.

Matcham, I., Savage, M.K., Gledhill, K.R., 2000. Distribution of seismic anisotropy in the subduction zone beneath the Wellington region, New Zealand. Geophys. J. Int. 140 (1), 1–10. https://doi.org/10.1046/j.1365-246x.2000.00928.x.

Mondal, P., Long, M.D., 2020. Strong seismic anisotropy in the deep upper mantle beneath the Cascadia backarc: Constraints from probabilistic finite-frequency SKS splitting intensity tomography. Earth Planet. Sci. Lett. 539, 116172.

Morley, A.M., Stuart, G.W., Kendall, J.M., Reyners, M., 2006. Mantle wedge anisotropy in the Hikurangi subduction zone, central North Island, New Zealand. Geophys. Res. Lett. 33 (5).

Nicol, A., Mazengarb, C., Chanier, F., Rait, G., Uruski, C., Wallace, L., 2007. Tectonic evolution of the active Hikurangi subduction margin, New Zealand, since the Oligocene. Tectonics 26 (4).

Nur, A., Simmons, G., 1969. Stress-induced velocity anisotropy in rock: an experimental study. J. Geophys. Res. 74 (27), 6667–6674.

Ohuchi, T., 2022. Grain-size-sensitive creep of olivine induced by oxidation of olivine in the Earth's deep upper mantle: Implications for weakening of the subduction interface. Phys. Earth Planet. Inter. 326, 106865 https://doi.org/10.1016/j.pepi.2022.106865.

Reyners, M., Eberhart-Phillips, D., Stuart, G., 2007. The role of fluids in lower-crustal earthquakes near continental rifts. Nature 446 (7139), 1075–1078.

Rümpker, G., Silver, P.G., 1998. Apparent shear-wave splitting parameters in the presence of vertically varying anisotropy. Geophys. J. Int. 135 (3), 790–800.

Russo, R.M., Silver, P.G., 1994. Trench-parallel flow beneath the Nazca plate from seismic anisotropy. Science 263 (5150), 1105–1111. https://doi.org/10.1126/science.263.5150.1105.

Salmon, M.L., Stern, T.A., Savage, M.K., 2011. A major step in the continental Moho and its geodynamic consequences: the Taranaki-Ruapehu line, New Zealand. Geophys. J. Int. 186, 32–44. https://doi.org/10.1111/j.1365-246X.2011.05035.x.

Savage, M.K., 1999. Seismic anisotropy and mantle deformation: what have we learned from shear wave splitting? Rev. Geophys. 37, 65–106.

Savage, M.K., Wessel, A., Teanby, N., Hurst, T., 2010. Automatic measurement of shear wave splitting and applications to time varying anisotropy at Mt. Ruapehu volcano, New Zealand. J. Geophys. Res. 115, B12321. https://doi.org/10.1029/2010JB007722.

Seward, A.M., Henderson, C.M., Smith, E.G.C., 2009. Models of upper mantle beneath the central North Island, New Zealand, from speeds and anisotropy of sub-horizontal P-waves (Pn). J. Geophys. Res.-Solid Earth 114, B01301. https://doi.org/10.1029/2008JB005805.

Sherburn, S., White, R.S., 2005. Crustal seismicity in Taranaki, New Zealand using accurate hypocentres from a dense network. Geophys. J. Int. 162 (2), 494–506. https://doi.org/10.1111/j.1365-246X.2005.02667.x.

Silver, P.G., 1996. Seismic anisotropy beneath the continents: probing the depths of geology. Annu. Rev. Earth Planet. Sci. 24, 385–432.

Silver, P.G., Chan, W.W., 1991. Shear wave splitting and subcontinental mantle deformation. J. Geophys. Res. 96 (B10), 16429. https://doi.org/10.1029/91jb00899.

Silver, P.G., Savage, M.K., 1994. The interpretation of shear-wave splitting parameters in the presence of two anisotropic layers. Geophys. J. Int. 119 (3), 949–963.

Stern, T., Stratford, W., Salmon, M., 2006. Subduction evolution and mantle dynamics at a continental margin: Central North Island, New Zealand. Rev. Geophys. 44, RG4002 https://doi.org/10.1029/2005RG000171.

Stern, T., Houseman, G., Salmon, M., Evans, L., 2013. Instability of a lithospheric step beneath western North Island, New Zealand. Geology 41 (4), 423–426.

Teanby, N., Kendall, J.M., Van der Baan, M., 2004. Automation of shear-wave splitting measurements using cluster analysis. Bull. Seismol. Soc. Am. 94 (2), 453–463. https://doi.org/10.1785/0120030123.

Townend, J., Sherburn, S., Arnold, R., Boese, C., Woods, L., 2012. Three-dimensional variations in present-day tectonic stress along the Australia–Pacific plate boundary in New Zealand. Earth Planet. Sci. Lett. 353, 47–59.

Uchida, N., Nakajima, J., Wang, K., Takagi, R., Yoshida, K., Nakayama, T., Hino, R., Okada, T., Asano, Y., 2020. Stagnant forearc mantle wedge inferred from mapping of shear-wave anisotropy using S-net seafloor seismometers. Nat. Commun. 11 (1), 5676.

Vecsey, L., Plomerová, J., Babuška, V., 2008. Shear-wave splitting measurements—Problems and solutions. Tectonophysics 462 (1–4), 178–196.

Walcott, R.I., 1984. The kinematics of the plate boundary zone throughNew Zealand: Acomparison of short- and long-term deformations. Geophys. J. Int. 79 (2), 613–633. https://doi.org/10.1111/j.1365-246X.1984.tb02244.x.

Walcott, R.I., 1987. Geodetic strain and the deformational history of the North Island of New Zealand during the late Cainozoic. Philosophical transactions of the Royal Society of London. Series A. Mathemat. Phys. Sci. 321 (1557), 163–181.

Wallace, L.M., Beavan, J., McCaffrey, R., Darby, D., 2004. Subduction zone coupling and tectonic block rotations in the North Island, New Zealand. J. Geophys. Res. Solid Earth 109 (B12). https://doi.org/10.1029/2004JB003241.

Walpole, J., Wookey, J., Kendall, J.M., Masters, T.G., 2017. Seismic anisotropy and mantle flow below subducting slabs. Earth Planet. Sci. Lett. 465, 155–167.

Wang, Z., Zhao, D., Chen, X., 2022. Seismic Anisotropy and Intraslab Hydrated Faults beneath the NE Japan Forearc. Geophys. Res. Lett. 49 (2) https://doi.org/10.1029/2021gl097266.

Wessel, A., 2010. Automatic Shear Wave Splitting Measurements at Mt. Ruapehu Volcano, New Zealand. Victoria University of Wellington (Master's thesis.).
Williams, C.A., Eberhart-Phillips, D., Bannister, S., Barker, D.H.N., Henrys, S., Reyners, M., Sutherland, R., 2013. Revised Interface Geometry for the Hikurangi Subduction Zone, New Zealand. Seismol. Res. Lett. 84 (6), 1066–1073. https://doi.org/10.1785/0220130035.
Wüstefeld, A., Bokelmann, G., 2007. Null Detection in Shear-Wave Splitting Measurements. Bull. Seismol. Soc. Am. 97 (4), 1204–1211. https://doi.org/10.1785/0120060190.
Wüstefeld, A., Bokelmann, G., Zaroli, C., Barruol, G., 2008. SplitLab: A shear-wave splitting environment in Matlab. Comput. Geosci. 34 (5), 515–528.
Yuan, H., & Romanowicz, B. (2010). Depth dependent azimuthal anisotropy in the western US upper mantle. Earth Planet. Sci. Lett., 300(3–4), 385–394.
Zal, H.J., 2020. Seismic Anisotropy and Velocity Structure in the North Island, New Zealand. Victoria University of Wellington (PhD's thesis.).